Chinese Chemical Letters 37 (2026) 112221

Contents lists available at ScienceDirect

Chinese Chemical Letters

journal homepage: www.elsevier.com/locate/cclet

Synergistically enhancing mechanochromism of carbazole derivatives *via* crystallization and host-guest complexation

Luyao Wang[a,1], Mengqi Pei[a,1], Dongdong Sun[a], Jingjing Liu[a], Xie Han[a,b,*], Simin Liu[a,b,*]

[a] School of Chemistry and Chemical Engineering, Wuhan University of Science and Technology, Wuhan 430081, China
[b] The State Key Laboratory of Refractories and Metallurgy, Institute of Advanced Materials and Nanotechnology, Wuhan University of Science and Technology, Wuhan 430081, China

ARTICLE INFO

Article history:
Received 13 July 2025
Revised 23 November 2025
Accepted 5 December 2025
Available online 6 December 2025

Keywords:
Cucurbit[*n*]urils
Mechanochromic luminescent
Confinement effect
Crystallization
Carbazole derivatives

ABSTRACT

Constructing high-contrast mechanochromic luminescent (MCL) materials with a wide range of emission color variations remains challenging. Herein, a host-guest strategy is proposed to optimize molecular MCL behavior. Two pyridinium-functionalized carbazole derivatives only exhibit a slight red-shifted fluorescence under mechanical stimulation. By forming host-guest complexes with cucurbit[*n*]urils (CB[*n*]s, $n = 8$ or 10), the complexes demonstrate more significant fluorescence wavelength changes after grinding. Mechanistic studies reveal that the crystallization and CB[*n*]'s confinement effect, synergistically induce more twisted molecular conformations and facilitate the planarization of guests under mechanical stimulation. Moreover, the host-guest complexes also exhibit outstanding MCL property in the polyvinyl alcohol (PVA) film. This strategy is both conceptually and synthetically simple and provides a promising method for preparing high-contrast MCL materials.

© 2026 Published by Elsevier B.V. on behalf of Chinese Chemical Society and Institute of Materia Medica, Chinese Academy of Medical Sciences.

Mechanochromic luminescent (MCL) materials, which exhibit emission color change in response to mechanical stimulus in solid state, have attracted much attention for their potential application in memory devices, sensors, security materials, and informational display areas [1–8]. In recent years, a large number of organic materials have been reported to show MCL behaviors. However, obtaining organic high-contrast MCL materials with wide-range fluorescence color change remains a challenging task [9–14]. Theoretically, molecular chemical structures are responsible for the MCL behavior of organic materials. Unfortunately, not all derivatives constructed based on a common molecular structural skeleton could exhibit similar excellent MCL performance, since the subtle change in molecular structure may lead to significant difference in MCL behavior [15–18]. On the other hand, polymorphism which endows a given compound with multiple crystalline states, has been used to enrich the fluorescence color changes of MCL materials [10,19–22]. The differences are primarily attributed to changes in molecular conformations and packing arrangements which have been proven to be main factors that influence MCL behaviors [5,8,19]. In other words, certain compounds may inherently possess high-contrast MCL properties, yet their optimal performance is obscured by unfavorable molecular conformations and packing arrangements. Developing an efficient method to modulate the molecular conformation or packing and realize the activation of high-contrast MCL behavior is of great significance.

Molecules based on an electron donor (D) and electron acceptor (A) have been proven to be prime candidates for the preparation of MCL materials by taking advantage of molecular conformation change [23–26]. Grinding can lead these molecules to change from twisted conformations to planar ones, accompanied by the emission color variation. Making the molecular conformation of the unground sample more twisted is significant for constructing high-contrast MCL materials. However, the tightly packed arrangement of D-A type molecules in the solid state often leads to planar molecular conformations.

In the field of supramolecular chemistry, various intermolecular interactions, including host-guest interactions, have been established as effective strategies for modulating molecular packing arrangements and conformations [27–29]. Cucurbit[*n*]urils (CB[*n*]s, $n = 5$–8, 10) as one kind of macrocyclic hosts exhibit high affinity toward organic cationic compounds in aqueous media [30–32]. By encapsulating guest molecules within their cavities, CB[*n*]s can effectively prevent the close packing between free guest molecules [33,34]. At the same time, CB[*n*]s can provide confined microenvironment to regulate the photophysical properties of the compounds [35–40]. Among these macrocyclic hosts, CB[8] and CB[10]

* Corresponding authors.
E-mail addresses: hanxie@wust.edu.cn (X. Han), liusimin@wust.edu.cn (S. Liu).
[1] These authors contributed equally to this work.

https://doi.org/10.1016/j.cclet.2025.112221
1001-8417/© 2026 Published by Elsevier B.V. on behalf of Chinese Chemical Society and Institute of Materia Medica, Chinese Academy of Medical Sciences.

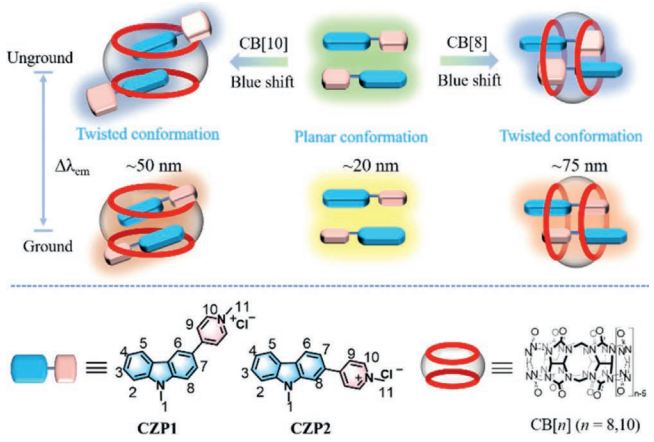


Fig. 1. The proposed host-guest complexation strategy for the construction of high-contrast MCL compounds; the molecular structures of **CZP1**, **CZP2**, and CB[*n*] (*n* = 8, 10).

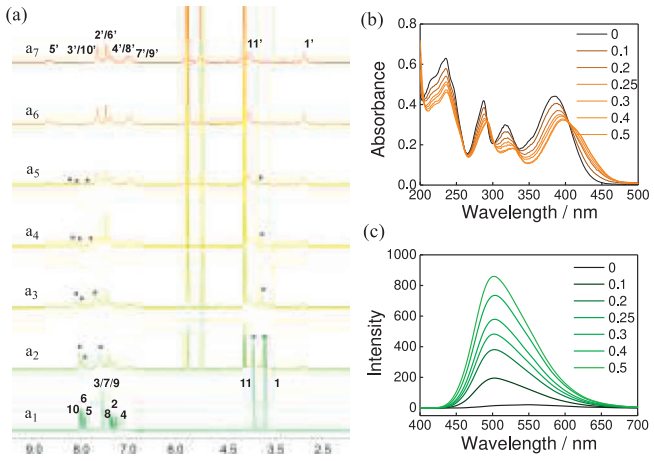


Fig. 2. (a) ^{1}H NMR spectra (600 MHz, D_2O, 298 K) for **CZP1** (2.0 mmol/L) with addition of different equivalents of CB[8] (a_1: 0, a_2: 0.1, a_3: 0.2, a_4: 0.25, a_5: 0.3, a_6: 0.4, a_7: 0.5; resonances of free guest **CZP1** are marked with *). (b) UV–vis absorption and (c) fluorescence spectra of **CZP1** (20 μmol/L) with addition of different equivalents of CB[8].

possess expanded cavity dimensions that facilitate the extension of guest molecular backbones, thereby enhancing the propensity for twisted conformational formation. It should be emphasized that not all guest molecules encapsulated within CB[*n*]s cavities exhibit significantly twisted conformations, as their three-dimensional structures are cooperatively governed by multiple intermolecular interactions. Notably, various host-guest interactions (such as hydrogen bonding, hydrophobic effects, ion-dipole interactions) provide the fundamental driving forces for such conformational modulation. Recently, we have proved that CB[8] can be used to realize the construction of a sequentially red-shifted mechanochromic system [41]. Such findings open new prospects for the modulation of MCL behaviors. On this basis, we designed and synthesized two guests (**CZP1** and **CZP2**) and investigated the influence of host-guest interaction on the MCL properties. The results revealed that CB[*n*]s can twist molecular conformation and activate the high-contrast MCL behaviors of D-A type molecules (Fig. 1).

The synthesis and characterization of **CZP1** and **CZP2** are shown in Supporting information. First, the host-guest complexation between **CZP1** and CB[*n*]s (*n* = 8, 10) in aqueous solution was investigated by ^{1}H NMR titration experiment and ESI-MS analysis. As shown in Fig. 2, upon the gradual addition of 0.5 equiv. CB[8] into the aqueous solution of **CZP1**, both free and bound proton signals of **CZP1** are observed, suggesting that the binding between CB[8] and **CZP1** is slow exchange kinetics on the ^{1}H NMR time scale. The proton signals of excess free guests exhibit a consecutive downfield shift with increasing amounts of CB[8]. Meanwhile, NMR experiments demonstrate that the signals of **CZP1** protons show obvious downfield shifts in the context of diluting concentrations (from 2 mmol/L to 0.2 mmol/L) (Fig. S1 in Supporting information). So the addition of CB[8] induced signal downfield shift of excess free guests may be attributed to the fact that the formation of host-guest complexes decreases the concentration of free guests, thus, the intermolecular π-π stacking interactions between the free guests are diminished [42]. Upon the addition of CB[8] (0.5 equiv.), signals of protons $H_{9,\ 10}$ on pyridinium and $H_{1,\ 6,\ 7}$ on carbazole unit are shifted upfield. Meanwhile, downfield shifts of $H_{4,\ 5}$ and H_{11} are observed (Fig. 2a_7), suggesting that the aromatic ring of pyridinium and partial carbazole unit are encapsulated into the cavity, while the methyl of pyridinium is located outside of CB[8] portals. Because of the slow exchange kinetics, the host-guest binding ratio is calculated as 1:2 according to integrals (Fig. S2 in Supporting information). At the same time, the observation of an ion peak at m/z = 937.84 corresponding to the 1:2 complex ([CB[8] + 2**CZP1**]$^{2+}$ = 937.54), proves the formation of 1:2 host-guest complex CB[8]·**CZP1**$_2$ (Fig. S3 in Supporting information). As shown in Fig. S4 (Supporting information), complexation between **CZP1** and CB[10] exhibits fast exchange kinetics on the ^{1}H NMR time scale. After the addition of the CB[10] host, the signals for guest protons became broad with significant upfield shifts, implying the encapsulation of **CZP1** molecule in CB[10]. ESI-MS evidenced the formation of CB[10]·**CZP1**$_2$ complex: The ion peak at m/z = 1103.88 corresponds to the 1:2 complex CB[10]·**CZP1**$_2$ ([CB[10] + 2**CZP1**]$^{2+}$ = 1103.64) (Fig. S5 in Supporting information).

Similar to that of **CZP1**, ^{1}H NMR experiments revealed that **CZP2** can form host-guest complex (CB[8]·**CZP2**$_2$) with CB[8] (Figs. S6 and S7 in Supporting information). Besides $H_{1,9,10}$ signals, the addition of CB[8] also leads H_{11} to undergo an upfield shift rather than a downfield shift, suggesting that the binding sites between CB[8] and the two guests (**CZP1**, **CZP2**) are different. For **CZP2**, the methyl on pyridinium can be encapsulated into the cavity of CB[8]. When CB[10] was added to the aqueous solution of **CPZ2**, lots of precipitates were formed and no signals were observed in the ^{1}H NMR spectra, suggesting the precipitation of host-guest complex.

As shown in Fig. 2b and Fig. S8a (Supporting information), upon adding CB[8] or CB[10] to the **CZP1** solution, the absorbance gradually decreases with bathochromic shift. Along with adding 0.5 equiv. of CB[8], a significant fluorescence blue shift to 516 nm with increased emission intensity is observed (λ_{max} of **CZP1** = 550 nm) (Fig. 2c). Similarly, addition of CB[10] also results in the hypsochromic shift of the emission wavelength and enhancement of the fluorescence intensity (Fig. S8b in Supporting information). The blue-shift of the fluorescence may be attributed to the lower polarity environment experienced by **CPZ1** in the cavity of CB[*n*] [43,44]. Encapsulating molecules inside the cavity of CB[*n*] can significantly restrict the intramolecular motions and suppress the non-radiative deactivation pathways of the excited state [45]. Thus, the photoluminescence quantum yield (Φ) of the solution increased remarkably from 1.67% (without CB[*n*]) to 43.21% (with 0.5 equiv. CB[8]) and 66.42% (with 0.5 equiv. CB[10]), respectively (Table S1 in Supporting information). Meanwhile, time-resolved luminescence spectra indicate that the emission lifetimes of free guests are much shorter than that of the complexes (Fig. S9 and Table S1 in Supporting information). This significant enhancement may be attributed to the CB[*n*]-induced restriction of the excited state deactivation and formation of dimers [46].

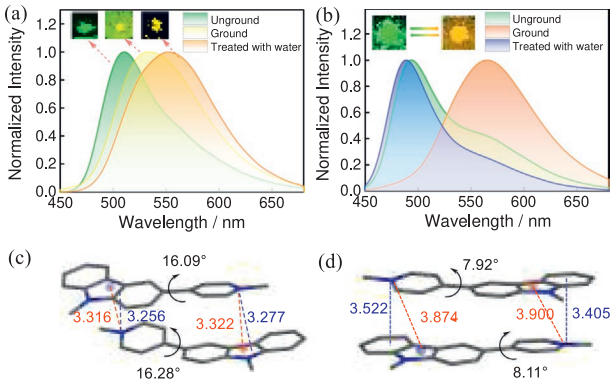


Fig. 3. Normalized fluorescent spectra of (a) **CZP1** and (b) CB[8]·**CZP1**$_2$ powder under different treatments. Insert: photographs of **CZP1** and CB[8]·**CZP1**$_2$ taken under irradiation at 365 nm. Molecular conformations of the dimer in the (c) CB[8]·**CZP1**$_2$ crystal and (d) **CZP1** crystal (d1: the distance from pyridinium cation to the center of carbazole unit; d2: the distance from pyridinium cation to the plane of carbazole unit). Hydrogen atoms are omitted in (c) and (d) for clarity.

The absorption and fluorescence spectra variation of **CZP2** in the presence of CB[8] are similar to that of **CZP1**. Binding with CB[8] results in the red-shift of the absorbance and the blue-shift of the emission (from 600 nm to 562 nm), respectively (Fig. S10 in Supporting information). The complexation-induced enhancement of fluorescence lifetime/quantum yield are also observed (Fig. S11 and Table S1 in Supporting information). As we know that CB[10] can only be dissolved in water by forming inclusion complexes with water-soluble guests [47]. Upon addition of CB[10] to the aqueous solution of **CZP2**, CB[10] initially dissolved, subsequently yielding yellow-green host-guest precipitates (**CZP2**⊂CB[10]) in the solution. Furthermore, SEM and TEM analyses reveal that the precipitates formed are octahedral nanoparticles (Fig. S12 in Supporting information).

Subsequently, the MCL properties of the guests and host-guest complexes were studied. As shown in Fig. 3a, **CZP1** powder exhibits green fluorescence peaking at 511 nm ($\tau = 9.10$ ns) with a shoulder peak at 555 nm ($\tau = 17.61$ ns, Table S2 and Fig. S13 in Supporting information), and the photoluminescence quantum yield is 37.83 %. After grinding, the maximum emission wavelength exhibits a bathochromic shift to 534 nm ($\Phi = 31.01$ %, $\tau = 11.08$ ns), accompanied by a fluorescence color change to yellow-green. When the ground sample is treated with water, the emission wavelength further red-shifts to 553 nm ($\Phi = 25.27$ %, $\tau = 31.96$ ns; Fig. S14 in Supporting information), closely matching the shoulder peak wavelength of the pristine powder. As shown in Fig. 3b, CB[8]·**CZP1**$_2$ powder (the solid samples were prepared by lyophilization) exhibits dual emission bands that peak at 493 and 565 nm ($\Phi = 54.43$ %, Table S2). The emission intensity of the higher energy emission band (493 nm, $\tau = 6.55$ ns) is much stronger than that of the lower energy emission band (565 nm, $\tau = 18.23$ ns, Fig. S15 and Table S2 in Supporting information), and the powder showed green fluorescence color under 365 nm light irradiation. Interestingly, compared with **CZP1**, grinding the complex results in a more remarkable fluorescence color and wavelength change (from green to orange, $\Delta\lambda = 75$ nm). The spectra reveal that the ground sample possesses only one red-shifted emission band at 568 nm ($\tau = 23.64$ ns, $\Phi = 45.09$ %, Table S2) which matches well with the lower energy emission band of the unground CB[8]·**CZP1**$_2$ powder. These results uncover that grinding the CB[8]·**CZP1**$_2$ complex can cause the emission intensity of the higher and lower energy emission bands to decrease and increase, respectively. Moreover, after soaking the ground solid in water, the original emission color of the complex is restored. As shown in Fig. S16 (Supporting information), the dual emission of CB[8]·**CZP1**$_2$ powder exhibits obvious excitation-wavelength dependence, suggesting that the lower energy emission band (565 nm) is derived from the intermolecular charge transfer effect [48]. Thus, the emission spectra change of CB[8]·**CZP1**$_2$ implied that the intermolecular charge transfer is enhanced after grinding. Moreover, solid-state UV–vis absorption spectral investigations demonstrate that a significant red-shift is observed after grinding the sample (Fig. S17 in Supporting information), suggesting the reinforced charge transfer effect.

To get a clear understanding of the MCL mechanisms, powder X-ray diffraction tests were performed. As shown in Fig. S18a (Supporting information), the crystalline structure of **CZP1** powder is slightly broken after grinding. Treating the ground solids with water results in the formation of a new crystalline state. However, different treatments can lead to a reversible morphology change of CB[8]·**CZP1**$_2$ between crystalline state and amorphous state (Fig. S18b in Supporting information). In order to get deeper insight into the molecular conformation and stacking characteristics of CB[8]·**CZP1**$_2$ complex, the crystal of CB[8]·**CZP1**$_2$ was studied. As illustrated in Fig. S19 (Supporting information), CB[8]·**CZP1**$_2$ crystals also exhibit dual emission bands with peaks at 485 and 560 nm. The intensity of the lower energy emission band is largely enhanced by grinding CB[8]·**CZP1**$_2$ crystals. The X-ray crystal structure of CB[8]·**CZP1**$_2$ complex reveals a 1:2 binding motif, in which two **CZP1** molecules stack in a head-to-tail manner in the cavity of a CB[8] host (Fig. S20a in Supporting information). Ion-dipole, C–H···π, and C–H···O interactions contribute to the stability of the complexes (Figs. S21-S23 in Supporting information). Moreover, the molecular conformations of the two guests in the cavity of CB[8] are not identical, the dihedral angles between the carbazole and pyridinium units are 16.09° and 16.28° (Fig. 3c), respectively. The pyridinium of one molecule is nearly parallel to the carbazole ring of the other molecule, and they are partially overlapped with each other. The distances between the pyridinium cations and the π systems of adjacent carbazole units are 3.316, 3.322 Å (d1) and 3.256, 3.277 Å (d2) (Fig. 3c), respectively. This molecular arrangement reveals the charge transfer interaction between the two guest molecules. Meanwhile, the **CZP1** molecules are separated in pairs by CB[8] hosts in the complexes, producing the discrete **CZP1** dimers (Fig. S24 in Supporting information). Thus, the MCL behavior of the complex may arise from the change in host-guest interactions, which induces a decrease in intermolecular distance or planarization of the molecular conformation in the dimer, further enhancing the intermolecular charge transfer effect [49,50].

As shown in Figs. S25 and S26 (Supporting information), grinding also lead to the enhancement of the charge transfer effect of **CZP1** powder. The crystal structure of **CZP1** reveals that two molecules stacked in a face-to-face motif and formed a dimer (Fig. S20b in Supporting information). The intramolecular dihedral angles between carbazole and pyridinium units are 7.92° and 8.11°, respectively (Fig. 3d), suggesting the more planar conformations compared to that of the guests in CB[8]·**CZP1**$_2$ crystal. Meanwhile, the distance from the pyridinium cations to the carbazole π systems in the dimers (d1 = 3.874, 3.900 Å and d2 = 3.522, 3.405 Å) tends to be farther in comparison to that of the guest dimers in CB[8]·**CZP1**$_2$ complex, implying that the intermolecular charge transfer effect in the dimers of **CZP1** crystal are weaker. Under the effect of multi kinds of intermolecular interactions (Fig. S27 in Supporting information), chloride ions are located between the two planes of the dimers (Fig. S28 in Supporting information), and they may work as steric hindrance units to restrict changes in molecular conformation and packing modes.

Collectively, these results reveal that the CB[8]-induced improvement of MCL behavior lies in two aspects. On one hand, CB[8] can endow **CZP1** molecules with more twisted conformations. On the other hand, discrete dimers can be formed by en-

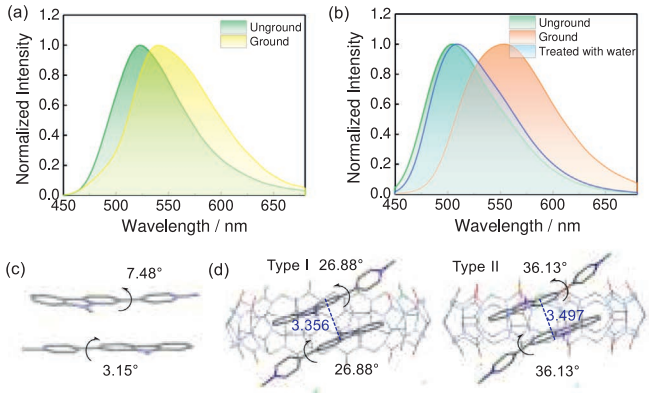


Fig. 4. Normalized fluorescent spectra of (a) **CZP2** and (b) CB[10]·**CZP2**$_2$ powder under different treatments. Molecular conformations of the dimer in the (c) **CZP2** and (d) CB[10]·**CZP2**$_2$ crystal. Hydrogen atoms are omitted in (c) and (d) for clarity.

capsulating **CZP1** molecules into the cavity of CB[8], and the steric hindrance effect (coming from the chloride ions) between the two planes of the dimer is eliminated. Thus, grinding can result in the efficiency enhancement of the emission coming from the intermolecular charge transfer effect. Meanwhile, the luminescence quantum yield of molecules is also important for the performance of mechanochromic materials. Although the quantum yields of the compounds reported here still lag behind some existing materials [51], it is noteworthy that the host-guest complexes exhibit higher quantum yields both before and after grinding compared to the free guests. This provides a feasible strategy for constructing mechanochromic materials with higher quantum yields.

Similarly, compared to **CZP2** molecules, **CZP2**⊂CB[10] complex also demonstrates a more significant wavelength red-shift after grinding (Figs. 4a and b). By treating these ground powders with water, the initial fluorescence color of **CZP2**⊂CB[10] is recovered, whereas **CZP2** just exhibits a decrease of fluorescence intensity (Fig. 4a and Fig. S29 in Supporting information). Photophysical parameters of **CZP2** and **CZP2**⊂CB[10] in different states are shown in Table S3 and Fig. S30 (Supporting information). PXRD analysis reveals that the reversible MCL behavior of **CZP2**⊂CB[10] and irreversible MCL behavior of **CZP2** relate to their distinct morphological transition (Fig. S31 in Supporting information). Moreover, the experimental XRD patterns of the **CZP2**⊂CB[10] complexes match the simulated patterns derived from the CB[10]·**CZP2**$_2$ single crystals (Fig. S31b), confirming that the precipitated product shares the same crystal lattice as the single crystals. This indicates that the **CZP2**⊂CB[10] complexes formed are indeed CB[10]·**CZP2**$_2$ complexes. As shown in Fig. S32 (Supporting information), pairwise anti-packed **CZP2** dimers are observed in the **CZP2** and CB[10]·**CZP2**$_2$ crystals. The intermolecular interactions of **CZP2** and CB[10]·**CZP2**$_2$ are shown in Figs. S33-S36 (Supporting information). Two types of inclusion complexes are observed in CB[10]·**CZP2**$_2$ crystals. Two **CZP2** guests stack together through $\pi\cdots\pi$ stacking interactions in the cavity of CB[10], and the molecular conformations of the guests are much more twisted than those in **CZP2** crystal (Figs. 4c and d). Moreover, formation of the host-guest complexes prevents the chloride ions from acting as steric hindrance units positioned between the two planes of the dimers (Fig. S37 in Supporting information). These variations follow a comparable pattern to the established contrast between **CZP1** and CB[8]·**CZP1**$_2$.

For **CZP1** and **CZP2** molecules, CB[8] and CB[10] can improve their MCL properties, respectively. However, CB[10]·**CZP1**$_2$ and CB[8]·**CZP2**$_2$ powder do not exhibit similar excellent MCL behaviors as CB[8]·**CZP1**$_2$ and CB[10]·**CZP2**$_2$ (Fig. S38 in Supporting information). This may be related to the different host-guest binding modes. On the other hand, the morphology of the solid is

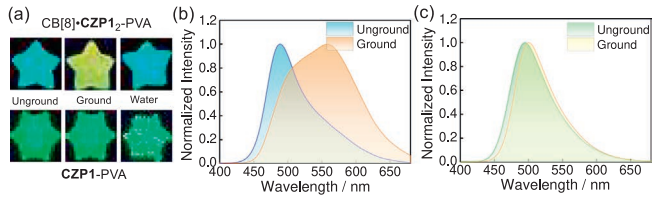


Fig. 5. Photographic images of (a) CB[8]·**CZP1**$_2$-PVA film and**CZP1**-PVA film under UV lamp. Normalized fluorescent spectra of (b) CB[8]·**CZP1**$_2$-PVA film and (c) **CZP1**-PVA film under different treatments.

an important factor to influence the MCL behavior. PXRD analysis revealed that both CB[10]·**CZP1**$_2$ and CB[8]·**CZP2**$_2$ powders are in amorphous states, in contrast to the crystalline states of CB[8]·CZP1$_2$ and CB[10]·CZP2$_2$. (Fig. S39 in Supporting information). For comparison, the MCL behavior of CB[8]·**CZP2**$_2$ crystal was investigated. The crystal structures are depicted in Fig. S40 (Supporting information). As shown in Fig. S41 (Supporting information), grinding CB[8]·**CZP2**$_2$ crystals induces an emission red-shift from 531 nm to 565 nm, differing markedly from its powder samples that in the amorphous state. These results imply that in addition to the cavity size of cucurbituril, the morphology of the host-guest complex in the solid state is also crucial. Therefore, we propose that the improved MCL properties are not only due to the confinement effect of the CB[*n*]'s cavities but also correlated with the well-ordered crystalline packing of the host-guest complexes in the solid state.

Next, **CZP1** and CB[8]·**CZP1**$_2$ molecules were doped into PVA films, and their MCL properties were investigated. As shown in Fig. 5, only CB[8]·**CZP1**$_2$-PVA film exhibits reversible color changes upon grinding and subsequently treating with water. Moreover, the fluorescence of CB[8]·**CZP1**$_2$-PVA is similar to that of CB[8]·**CZP1**$_2$ powder, implying that CB[8] can work as a "molecular conformation and packing protector" to prevent the dimeric structure of **CZP1** guests from being largely destroyed in PVA film. At the same time, the intermolecular interactions between CB[8]·**CZP1**$_2$ complex and PVA may also take part in influencing the molecular conformation of the complexes, thereby enabling the grinding-induced fluorescence change.

In summary, we have improved the MCL properties of pyridinium-functionalized carbazole derivatives through a host-guest inclusion strategy. Compared to **CZP1** and **CZP2**, CB[8]·**CZP1**$_2$ and CB[10]·**CZP2**$_2$ exhibit optimized MCL properties. Further analysis revealed that the confinement effect of CB[*n*]s induces more twisted conformations in the guest molecules and shields the steric hindrance from chloride ions, leading to a more significant enhancement of charge transfer effect under mechanical stimulation. Notably, crystalline effect is critical in maintaining well-ordered molecular packing of the complexes, which is essential for the improved MCL behavior. Furthermore, CB[8] functions as a "molecular conformation and packing protector" in polymer films, enabling the fabrication of high-contrast MCL film materials. Our findings demonstrate the potential of this host-guest inclusion strategy for constructing high-contrast MCL materials.

CRediT authorship contribution statement

Luyao Wang: Writing – original draft, Methodology, Investigation, Data curation. **Mengqi Pei:** Writing – original draft, Methodology, Investigation, Data curation. **Dongdong Sun:** Data curation. **Jingjing Liu:** Data curation. **Xie Han:** Writing – review & editing, Project administration, Conceptualization. **Simin Liu:** Writing – review & editing, Project administration, Conceptualization.

Declaration of competing interest

The authors declare that they have no known competing financial interests or personal relationships that could have appeared to influence the work reported in this paper.

Acknowledgments

This work was financially supported by the National Natural Science Foundation of China (No. 21901194). Prof. X. Liu (Singapore University of Technology and Design) is gratefully acknowledged for the data analysis in this study.

Supplementary materials

Supplementary material associated with this article can be found, in the online version, at doi:10.1016/j.cclet.2025.112221.

References

[1] F. Ciardelli, G. Ruggeri, A. Pucci, Chem. Soc. Rev. 42 (2013) 857–870.
[2] Z. Chi, X. Zhang, B. Xu, et al., Chem. Soc. Rev. 41 (2012) 3878–3896.
[3] H. Sun, S. Liu, W. Lin, et al., Nat. Commun. 5 (2014) 3601.
[4] Z. Ma, Z. Wang, M. Teng, et al., ChemPhysChem 16 (2015) 1811–1828.
[5] Y. Sagara, S. Yamane, M. Mitani, et al., Adv. Mater. 28 (2015) 1073–1095.
[6] P. Xue, J. Ding, P. Wang, et al., J. Mater. Chem. C 4 (2016) 6688–6706.
[7] K. Wang, L. Wan, J. Wang, et al., Chin. Chem. Lett. 35 (2024) 109554.
[8] Q. Li, Z. Li, Acc. Chem. Res. 53 (2020) 962–973.
[9] J. Zhang, M. Zhu, Y. Lu, et al., Chem. Eur. J. 28 (2022) e202200458.
[10] W. Wang, R. Li, S. Xiao, et al., CCS Chem. 4 (2022) 899–909.
[11] Z. Lv, Z. Man, Z. Xu, et al., Adv. Opt. Mater. 9 (2021) 2100598.
[12] C. Zhu, Q. Luo, Y. Shen, et al., Angew. Chem. Int. Ed. 60 (2021) 8510–8514.
[13] W.Z. Yuan, Y. Tan, Y. Gong, et al., Adv. Mater. 25 (2013) 2837–2843.
[14] W. Guo, M. Wang, L. Si, et al., Chem. Sci. 14 (2023) 6348–6354.
[15] T. Jadhav, B. Dhokale, R. Misra, J. Mater. Chem. C 3 (2015) 9063–9068.
[16] K. Zheng, H. Chen, Y. Xiao, et al., Chem. Eur. J. 27 (2021) 14964–14970.
[17] X. Huang, L. Qian, Y. Zhou, et al., J. Mater. Chem. C 6 (2018) 5075–5096.
[18] S. Nagai, M. Yamashita, T. Tachikawa, et al., J. Mater. Chem. C 7 (2019) 4988–4998.
[19] C. Wang, Z. Li, Mater. Chem. Front. 1 (2017) 2174–2194.
[20] B. Fang, M. Chu, Z. Wu, et al., J. Mater. Chem. C 7 (2019) 4434–4440.
[21] F. Hu, W. Yang, L. Li, et al., Chem. Eng. J. 464 (2023) 142678.
[22] Z. Wang, M. Wang, J. Peng, et al., J. Phys. Chem. C 123 (2019) 27742–27751.
[23] X.Y. Shen, Y.J. Wang, E. Zhao, et al., J. Phys. Chem. C 117 (2013) 7334–7347.
[24] R. Pashazadeh, G. Sych, S. Nasiri, et al., Chem. Eng. J. 401 (2020) 125962.
[25] A. Li, N. Chu, J. Liu, et al., Mater. Chem. Front. 3 (2019) 2768–2774.
[26] H.X. Yu, J. Zhi, T. Shen, et al., J. Mater. Chem. C 7 (2019) 8888–8897.
[27] G. Wu, F. Li, B. Tang, et al., J. Am. Chem. Soc. 144 (2022) 14962–14975.
[28] R. Wang, H. Deng, W. Cheng, et al., Dyes Pigments 235 (2025) 112578.
[29] J.R. Wu, G. Wu, D. Li, et al., Angew. Chem. Int. Ed. 62 (2023) e202218142.
[30] S.J. Barrow, S. Kasera, M.J. Rowland, et al., Chem. Rev. 115 (2015) 12320–12406.
[31] J. Lagona, P. Mukhopadhyay, S. Chakrabarti, et al., Angew. Chem. Int. Ed. 44 (2005) 4844–4870.
[32] X. Yang, F. Liu, Z. Zhao, et al., Chin. Chem. Lett. 29 (2018) 1560–1566.
[33] Y. Jiao, K. Liu, G. Wang, et al., Chem. Sci. 6 (2015) 3975–3980.
[34] F. Biedermann, E. Elmalem, I. Ghosh, et al., Angew. Chem. Int. Ed. 51 (2012) 7739–7743.
[35] H. Nie, Z. Wei, X.L. Ni, et al., Chem. Rev. 122 (2022) 9032–9077.
[36] R.N. Dsouza, U. Pischel, W.M. Nau, Chem. Rev. 111 (2011) 7941–7980.
[37] L. Mao, S. Li, X. Zhang, et al., Chin. Chem. Lett. 35 (2024) 109363–109373.
[38] X.K. Ma, Y. Liu, Acc. Chem. Res. 54 (2021) 3403–3414.
[39] G. Wu, Y.W. Yang, Cell Rep. Phys. Sci. 5 (2024) 101873–101886.
[40] C. Yin, Z.A. Yan, X. Ma, Chem. Commun. 59 (2023) 13421–13433.
[41] D. Sun, Y. Wu, X. Han, et al., Nat. Commun. 14 (2023) 4190.
[42] S. Kuang, Z. Hu, H. Zhang, et al., Chem. Commun. 54 (2018) 2169–2172.
[43] M. Megyesi, L. Biczók, I. Jablonkai, J. Phys. Chem. C 112 (2008) 3410–3416.
[44] Y. Gu, Z. Zhao, H. Su, et al., Chem. Sci. 9 (2018) 6497–6502.
[45] D. Sun, Y. Wu, X. Han, et al., Chem. Eur. J. 27 (2021) 16153–16160.
[46] G. Wu, Y.J. Bae, M. Olesińska, et al., Chem. Sci. 11 (2020) 812–825.
[47] J. Yang, X. Hu, M. Fan, et al., Org. Chem. Front. 10 (2023) 422–429.
[48] X.H. Jin, C. Chen, C.X. Ren, et al., Chem. Commun. 50 (2014) 15878–15881.
[49] Y. Liu, Q. Zeng, B. Zou, et al., Angew. Chem. Int. Ed. 57 (2018) 15670–15674.
[50] J. Liu, Y. Zhang, K. Zhang, et al., Org. Electron. 71 (2019) 212–219.
[51] Y. Guo, A. Wu, Q. Zhang, et al., Chem. Eng. J. 497 (2024) 154721.